energies

MDPI

Article

Stability and Control for Buck–Boost Converter for Aeronautic Power Management

Antonio Russo * and Alberto Cavallo

Dipartimento di Ingegneria, Università degli Studi della Campania "Luigi Vanvitelli", 81031 Aversa, Italy
* Correspondence: antonio.russo1@unicampania.it

Abstract: The need for greener and cleaner aviation has accelerated the transition towards more electric systems on the More Electric Aircraft. One of the key challenges related to the increasing number of electrical devices onboard is the control of bidirectional power converters. In this work, stability analysis and control of a buck–boost converter for aeronautic applications are presented. Firstly, stability of the buck–boost converter in the Lyapunov sense is proven by resorting to input-to-state stability notions. Then, a novel control design based on second order sliding mode control and uniting control, aimed at overcoming the difficulties generated by the nonlinear input gain function of the system not being sign definite, is presented. Extensive and detailed simulations, designed to emulate one of the possible energy management policies onboard a More Electric Aircraft, confirm the correctness of the theoretical analysis both in buck and in boost mode.

Keywords: sliding mode control; power converters; aeronautic application; energy management

Citation: Russo, A.; Cavallo, A. Stability and Control for Buck–Boost Converter for Aeronautic Power Management. *Energies* **2023**, *16*, 988. https://doi.org/10.3390/en16020988

Academic Editor: Ali Mehrizi-Sani

Received: 15 December 2022
Revised: 10 January 2023
Accepted: 14 January 2023
Published: 16 January 2023

1. Introduction

In the last two decades, the idea of increasing the number of electric devices onboard aircraft has gained more and more popularity. The initial motivation was to replace hydraulic and pneumatic actuators with electric ones, thus increasing efficiency and safety onboard, and possibly reducing weight. This rationale gave birth to the so-called More Electric Aircraft (MEA) paradigm [1], on which different national and international projects have been funded. For instance, since the Fifth Framework Programme dating back to the beginning of 2000s (e.g., with the project Power Optimised Aircraft, POA [2]), the European Community has constantly increased the budget for aerospace-oriented projects, with emphasis on employing electric technologies onboard. Since the beginning of 2010s, the creation of the "Clean Sky JU" initiative [3] has increased the focus on noise and weight reduction. It is worth citing that recently the more ambitious project of an All Electric Aircraft (AEA) has been gaining more interest. For instance, some months ago, Hyundai promised to launch an all-electric flying taxi in 2028 to reduce gas emission and congestion in urban traffic [4].

From a technical point of view, what really motivates the use of electric actuators in the MEA approach is their efficiency. Pneumatic power, used mainly in wings ice protection systems and in environmental control systems results in poor efficiency and complex maintenance [5]. On the other hand, hydraulic actuators are robust and able to produce high power, but they are generally heavy and subject to leakage of corrosive liquids [5]. Moreover, the price paid when transferring mechanical energy from the main energy source (usually, the aircraft gas turbine engine) to the loads (e.g., fuel and oil pumps) is the usage of heavy gearbox systems [6,7]. It is apparent that it is possible to improve efficiency by directly using electrically fed devices, e.g., electric pumps for fuel, electrically driven air compressors, and so on. Incidentally, this also increases robustness to faults and allows capabilities of fault detection and diagnosis at the system level.

The increase of electrically operated devices onboard requires advanced automatic control of the electric network since it is no longer possible for the pilot to manually control

devices that have to be operated in a coordinated fashion. Moreover, employing automatic control avoids human errors and/or misunderstanding and increases reliability. Actually, two levels of control have to be considered, namely a low-level control addressing the single electric device to be operated and a high-level supervisory control coordinating the network of low-level controllers according to prescribed requirements or control objectives. Possible control objectives are optimal distribution of electric power, reduction of weights onboard, alleviation of stresses on generators (e.g., by smoothening power peaks), optimal response to time-varying loads, and so on. This is possible if the electric actuators are transformed into "smart" devices by a low-level controller acting on the power converters feeding the actuator, which is the interface between the actuator and the electric network. Hence, bidirectional power converters capable of four-quadrant operations are key elements of the MEA paradigm as they act as a bridge between the main aircraft bus and auxiliary power sources, such as batteries or supercapacitors. For instance, the presence of auxiliary batteries is exploited to implement load-sharing policies between the aircraft generator and the battery itself to allow the installation of smaller, thus lighter, onboard generators [8,9]. Supercapacitors, instead, can be adopted for their intrinsic capability to absorb or provide fast power peaks, thus allowing stress reduction on the mechanical parts of the aircraft generator [10,11].

The power flow between the main aircraft bus and the battery (and/or supercapacitors) is regulated by bidirectional four-quadrant power converters [12,13]. A converter for this application has to meet the prevalent aeronautic requirements, such as being a low-cost design and minimizing the component size, weight, and number. Fixed-frequency operation is desired to meet electromagnetic interference (EMI) standards ,and a highly compact design and a low overall weight are required. Efficiency of the dc–dc converter over a wide input and output power range is also a critical issue since the converter is required to work at different operating points. One commonly used converter topology for this application, due to its limited number of components and high efficiency, is the four switches buck–boost converter, which is adopted in this work. As highlighted in [14], there are a number of alternatives to the four-switches buck–boost converter, such as the constant-frequency zero-current-switching quasi-square-wave (CF-ZVS-QSC) converter [15], the single ended primary inductor converter (SEPIC) [16,17], or the zero-voltage zero-current switching (ZVZCS) converter presented in [17]. The main drawbacks of these converters are doubled switch-blocking voltage stress and diode recovery losses in case of the SEPIC [17], a larger number of passive components, and a larger inductance value for the main inductor in the SEPIC and ZVZCS topology [15]. Furthermore, SEPIC and ZVZCS use a capacitive energy transfer that performs badly in high-power applications. Other drawbacks of resonant converters are variable switching frequency, which complicates EMI filter design, and limitations in operating range for soft switching.

The standard strategy in controlling power converters is to consider a linear (typically, a proportional–integral PI or proportional–integral–derivative PID) controller. This is justified by a preliminary linearisation of the mathematical model of the network, device, and converter around a prescribed operating point. However, if the operating point drastically changes (e.g., due to a load change), there is no guarantee that the linear controller still behaves correctly, and even stability may be lost, as is well-known, for instance, in the presence of constant power load (CPL) [18–21]. Note that often the action of low-level controllers is to exactly make the load a CPL; hence the risk of destabilising the electric network is a critical issue. For this reason, nonlinear controllers able to directly address the nonlinear nature of the controlled electrical network, thus avoiding linearisation, are becoming more common [22,23].

1.1. Contributions

In this paper, the control problem of a standard aeronautic electric network comprising a high-voltage DC (HVDC) generator and a low-voltage DC (LVDC) battery is considered. Usually, the HVDC is found in an aircraft gas turbine engine acting as an AC electric

generator and followed by a voltage rectification stage. As mentioned above, the key element to control is the DC/DC converter that acts as an interface between HVDC and LVDC busses. By using a suitable control strategy, it is possible to accurately impose the flow of energy both from the generator to the battery (thus recharging the battery) and from the battery to the HVDC, thus helping the generator if some extra load requires more power than the rated generator power. In this work, a buck–boost converter is considered and stability analysis and control design are thoroughly addressed. Specifically, stability in the Lyapunov sense is proved resorting to the notion of Input-to-State Stability [24], while the control design is carefully addressed for the buck and the boost mode based on saturated Suboptimal Second Order Sliding Mode Control (SOSMC) [25]. In fact, it is observed that while the boost mode satisfies the required assumptions for SOSMC implementation, the *nonlinear input gain function* in buck mode is not sign definite, thus not enabling direct application of the SOSMC. In fact, the nonlinear input gain being sign definite is a fundamental hypothesis in most sliding mode algorithms [26]. As a solution to this challenge, a switching control strategy inspired by *uniting control* [27] has been designed and implemented. This technique is particularly indicated for systems characterized by difficulties (or the impossibility) in the design of a unique controller capable of guaranteeing stability, performance, and robustness. For instance, a recent application of uniting control was presented in [28] for the case of stabilization on $\mathcal{S}^1$ space. Furthermore, the adopted SOSMC also takes into account the duty cycle characteristic to be constrained in the interval [0,1] [29].

Finally, the main contributions of this work can be summarized in the following points:

- The stability of the buck–boost converter is addressed and demonstrated through the ISS framework;
- A (monotonic) Saturated Suboptimal Second Order Sliding Mode Control is designed to achieve finite time control of the converter current to the given reference;
- The overall designed control architecture is designed as the combination of the (monotonic) Saturated Suboptimal Second Order Sliding Mode Control and a feedback-based monotonic control algorithm. The two control laws are then orchestrated through a switching control strategy based on uniting control. Here, monotonicity is fundamental to avoid repetitive switching among the two control laws.

1.2. Structure of the Paper

After the Introduction, the electrical network that synthetically describes the aeronautic power grid is presented in Section 2 together with the dynamic equations describing the grid behavior. Stability analysis and converter control design are presented in Sections 3 and 4, respectively. In Section 5, the outcome of the proposed control strategy is presented in a detailed simulation environment, while conclusions are drawn in Section 6, with a list of symbols afterwards.

2. The Electrical Network

The schematic of the electrical network that describes the aeronautic power grid is shown in Figure 1. The DC aircraft electric generator is modeled as an ideal voltage source, V_{net}, with internal resistance ESR_{net}, while, the DC aircraft battery is represented here as an ideal voltage source, V_{batt}, with internal resistance ESR_{batt}. Aeronautical loads connected on the network side can be modeled as a time-varying resistor denoted by R_D. As we are interested in active power, only resistive loads will be considered in this work. Connecting the two power sources, there is a four-switch buck–boost bidirectional converter, where the switches Q_1 and Q_2 operate in anti-phase as well as the two switches Q_3 and Q_4. Such switches are controlled by Pulse Signal Modulation (PWM) signal generators driven by the duty cycle signals d_1 and d_2, the former regulating switches Q_1 and Q_2, the latter regulating switches Q_3 and Q_4. The converter comprises two capacitors, namely C_1 and C_2 and an inductor, L, and we indicate the generator current with ι_{gen} and the battery current with ι_{batt}.

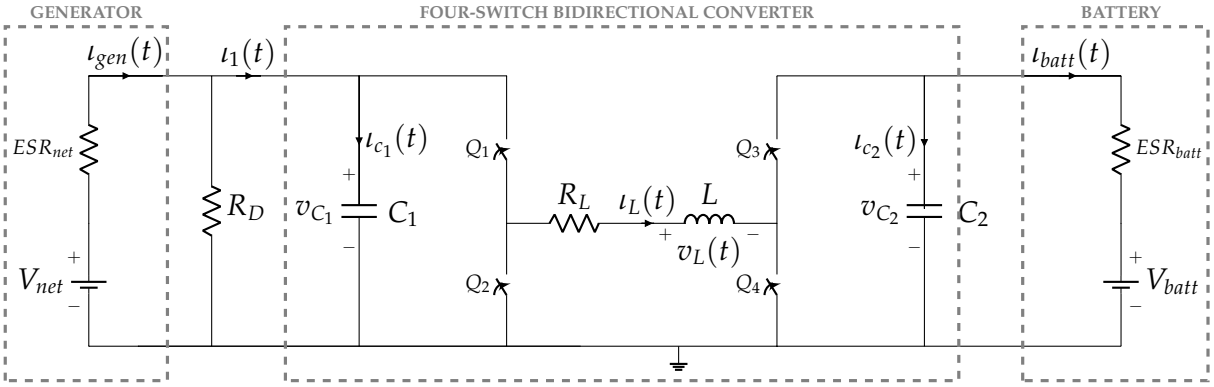

Figure 1. Schematic of the electrical power grid.

Considering the four possible configurations of the switches, namely:

- Q_1 ON, Q_2 OFF, Q_3 ON, and Q_4 OFF,
- Q_1 OFF, Q_2 ON, Q_3 ON, and Q_4 OFF,
- Q_1 ON, Q_2 OFF, Q_3 OFF, and Q_4 ON,
- Q_1 OFF, Q_2 ON, Q_3 OFF, and Q_4 ON,

different operating principles can be observed. The converter will operate as a traditional synchronous boost if switch Q_1 keeps the ON state and Q_2 keeps the OFF state, while Q_3 and Q_4 have a switching behavior. Similarly, it operates as synchronous buck when keeping Q_3 ON and Q_4 OFF, while Q_1 and Q_2 are switching. Specifically, when Q_1 and Q_3 are turned on and Q_2 and Q_4 are turned off, the inductor gets charged during buck mode, while it discharges the stored energy during boost mode. When Q_1 and Q_4 are turned on and Q_2 and Q_3 are turned off, the inductor is charged during boost mode. Instead, when Q_2 and Q_3 are turned on and Q_1 and Q_4 are turned off, the inductor discharges energy during buck mode. Finally, the case when Q_2 and Q_4 are turned on and Q_1 and Q_3 are turned off is utilized in neither buck nor boost mode, but only when the converter needs to be disconnected from the grid for safety reasons [13].

Considering the four possible configurations of the switches, it is not difficult to derive the set of four topologies (and the corresponding sets of linear differential equations), each one describing a specific configuration. The power grid dynamic equations can be written in a compact way as follows:

$$\begin{aligned}\begin{bmatrix}\dot{v}_{C_1}\\ i_L\\ \dot{v}_{C_2}\end{bmatrix} &= \begin{bmatrix}-\left(\frac{1}{ESR_{net}}+\frac{1}{R_D}\right)\frac{1}{C_1} & 0 & 0\\ 0 & -\frac{R_L}{L} & 0\\ 0 & 0 & -\frac{1}{ESR_{batt}C_2}\end{bmatrix}\begin{bmatrix}v_{C_1}\\ \iota_L\\ v_{C_2}\end{bmatrix}+\begin{bmatrix}0 & -\frac{1}{C_1} & 0\\ \frac{1}{L} & 0 & 0\\ 0 & 0 & 0\end{bmatrix}\begin{bmatrix}v_{C_1}\\ \iota_L\\ v_{C_2}\end{bmatrix}d_1+\\ &+\begin{bmatrix}0 & 0 & 0\\ 0 & 0 & -\frac{1}{L}\\ 0 & \frac{1}{C_2} & 0\end{bmatrix}\begin{bmatrix}v_{C_1}\\ \iota_L\\ v_{C_2}\end{bmatrix}d_2+\begin{bmatrix}\frac{V_{net}}{ESR_{net}C_1}\\ 0\\ \frac{V_{batt}}{ESR_{batt}C_2}\end{bmatrix}.\end{aligned} \tag{1}$$

Let us define the state vector $x \coloneqq [x_1, x_2, x_3]^\top = \left[v_{C_1}, \iota_L, v_{C_2}\right]^\top$, where x_1 is the voltage across the capacitor C_1, x_2 is the current flowing through the inductor L (characterized by inner resistance R_L), and x_3 is the voltage across the capacitor C_2.

Therefore, system (1) can be reorganized as

$$\dot{x} = Ax + B_1 x d_1 + B_2 x d_2 + \Gamma, \qquad (d_1, d_2) \in [0,1] \times [0,1]. \tag{2}$$

The main objective of the bidirectional converter is to regulate the power flow between the main aeronautical bus and the battery side. Several objectives can be achieved through regulation of the power flow, for instance: regulation of the bus side voltage in case of generator failure, control of converter input current in order to limit the generator current below a given critical value, or recharge the battery in constant current or constant power

mode. In this paper, the control of converter input current ι_1, aimed at generator current limitation, is tackled. Such a challenge can be described as the problem of regulating current $\iota_1(t)$, indicated in Figure 1 and calculated as

$$\iota_1(t,x) = \frac{V_{net}}{ESR_{net}} - x_1(t)\left(\frac{1}{ESR_{net}} + \frac{1}{R_D}\right), \tag{3}$$

to a given piecewise constant reference current $\bar{\iota}_1$.

This control objective can be achieved by properly regulating the duty cycle signals d_1 and d_2. Several modulation strategies are available for the control of the class of bidirectional converters as in Figure 1, e.g., hard-switching and soft-switching [30]. In the case of hard-switching, the two legs commute alternatively, that is d_1 is kept to 1, d_2 operates in boost mode and operates, d_2 is kept to 1, and d_1 operates in buck mode. The soft-switching modulation is instead characterized by the simultaneous switching of the two legs. As detailed in [31], where a similar application is investigated with a focus on the network parameters optimization, both modulation strategies have their pros and cons; however, hard-switching is preferred over soft-switching modulation because of its lower losses. For this reason, also in this work hard-switching modulation is considered.

3. System Stability

In this section, it will be formally proven that system (2) cannot undergo any unstable behavior despite the selected control law (note that here the instability notion is intended in the sense of Lyapunov [32]). This result is achieved by resorting to the concept of *Input-to-State Stability* (ISS). Preliminarily, let us recall the definition of ISS and its Lyapunov characterization, where comparison function definitions from [32] are adopted.

Definition 1 (Input-to-State Stability [24]). *The system*

$$\dot{x}(t) = f(t,x,u) \tag{4}$$

with $f : \mathbb{R}_{\geq 0} \times \mathbb{R}^n \times \mathbb{R}^m$, piecewise continuous in t and locally Lipschitz in x and u, is said to be ISS if there exist a class $\mathcal{KL}$ function β and a class $\mathcal{K}$ function γ, such that, for any initial state $x(t_0)$ and any bounded input $u(t)$, the solution $x(t)$ exists for all $t \geq t_0$ and satisfies

$$|x(t)| \leq \beta(|x(t_0)|, t - t_0) + \gamma\left(\sup_{t_0 \leq \tau \leq t} |u(\tau)|\right) \tag{5}$$

Definition 1 provides an estimation of the bound of the system state norm provided that the input norm is bounded. The bound depends on the sum of two terms, the first depending on the initial condition of the system and decreasing with time, while the second depends on the input infinite norm. A sufficient condition for the ISS property is given by the following Lyapunov-like theorem [24].

Theorem 1 (ISS Lyapunov Characterization [24]). *Consider system (4), and let $V : \mathbb{R}_{\geq 0} \times \mathbb{R}^n \to \mathbb{R}$ be a continuously differentiable function, such that*

$$\alpha_1(|x|) \leq V(t,x) \leq \alpha_2(|x|) \tag{6}$$

$$\frac{\partial V}{\partial t} + \frac{\partial V}{\partial x} f(x,u,t) \leq -\alpha(|x|) + \chi(|u|), \tag{7}$$

holds for all $(t,x,u) \in \mathbb{R}_{\geq 0} \times \mathbb{R}^n \times \mathbb{R}^m$, where α_1, α_2, α are class $\mathcal{K}_\infty$ functions, and χ is a class $\mathcal{K}$ function. Then, system (4) is ISS.

It is now possible to characterize the stability of system (2) with respect to its uncontrolled input Γ. This stability result is summarized in the following theorem.

Theorem 2 (**ISS Property of System** (2))**.** *The switched system* (2) *is ISS with respect to the uncontrolled input vector* Γ *for any arbitrary switching signal.*

Proof. In order to prove the theorem statement, a reasonable choice for the Lyapunov function is the system energy function, that is

$$V(x) = \frac{1}{2}(C_1 v_{C_1}^2 + L\iota_L^2 + C_2 v_{C_2}^2) = \frac{1}{2}(C_1 x_1^2 + L x_2^2 + C_2 x_3^2). \tag{8}$$

Its time derivative along the trajectory of system (2) is

$$\begin{aligned} \dot{V}(x) &= C_1 x_1 \dot{x}_1 + L x_2 \dot{x}_2 + C_2 x_3 \dot{x}_2 \\ &= -\left(\frac{1}{R_D} + \frac{1}{ESR_{net}}\right) x_1^2 - R_L x_2^2 - \frac{x_3^2}{ESR_{batt}} + \frac{V_{net}}{ESR_{net}} x_1 + \frac{V_{batt}}{ESR_{batt}} x_3. \end{aligned} \tag{9}$$

Consider the property for the square of a binomial $a^2 + b^2 \geq \pm 2ab$, and apply it to the last two terms of (9). More precisely, it holds that

$$\frac{V_{net}}{ESR_{net}} x_1 \leq \frac{1}{4} \frac{x_1^2}{ESR_{net}} + \frac{V_{net}^2}{ESR_{net}} \quad \text{and} \quad \frac{V_{batt}}{ESR_{batt}} x_3 \leq \frac{1}{4} \frac{x_3^2}{ESR_{batt}} + \frac{V_{batt}^2}{ESR_{batt}}$$

Therefore, the time derivative of the Lyapunov function is bounded by

$$\dot{V}(x) \leq -\left(\frac{1}{R_D} + \frac{3}{4ESR_{net}}\right) x_1^2 - R_L x_2^2 - \frac{3}{4ESR_{batt}} x_3^2 + \frac{V_{net}^2}{ESR_{net}} + \frac{V_{batt}^2}{ESR_{batt}} \tag{10}$$

which implies that system (2) is ISS with respect to the input Γ with

$$\begin{aligned} &\alpha_1(|x|) = \frac{1}{4}(C_1 x_1^2 + L x_2^2 + C_2 x_3^2), \quad \alpha_2(|x|) = (C_1 x_1^2 + L x_2^2 + C_2 x_3^2), \\ &\alpha(|x|) = \left(\frac{1}{R_D} + \frac{3}{4ESR_{net}}\right) x_1^2 + R_L x_2^2 + \frac{3}{4} \frac{x_3^2}{ESR_{batt}}, \quad \chi(|\Gamma|) = \frac{V_{net}^2}{ESR_{net}} + \frac{V_{batt}^2}{ESR_{batt}}. \end{aligned}$$

□

The ISS proof for system (2) has dual importance. Firstly, it can be seen that the time derivative of the selected Lyapunov function does not depend on the input terms d_1 and d_2. This, in turn, implies that stability of the system (intended as boundedness) is not affected by the duty cycle trajectories $d_1(t)$ and $d_2(t)$. Secondly, having proved the ISS property implies that the norm of the system state is bounded with a bound dependent on the norm of Γ. This means that there exist positive scalars X_1^-, X_1^+, X_2^+, X_3^-, X_3^+ and a negative scalar X_2^-, such that $x_1 \in [X_1^-, X_1^+]$, $x_2 \in [X_2^-, X_2^+]$, and $x_3 \in [X_3^-, X_3^+]$. Note that positivity of X_1^- and X_3^- is not directly implied by the ISS property, but it is merely based on physical and application considerations (in fact, x_1 and x_3 represent capacitor voltages and can be assumed to be always positive). Hereafter, we will indicate with $\mathcal{D}$ the set containing the state trajectories, that is $\mathcal{D} := [X_1^-, X_1^+] \times [X_2^-, X_2^+] \times [X_3^-, X_3^+]$.

Remark 1. *As described in [24], the ISS property of system (2) could have been equivalently demonstrated by proving that: (1) system (2) is zero globally asymptotically stable (0-GAS) and (2.i) system (2) has the asymptotic gain property (AG) or (2.ii) system (2) has the limit property (LIM). However, while verification of the 0-GAS property is trivial (note that the unforced system is linear), proving AG or LIM for system (2) is more complex than the proof provided in Theorem 2.*

As a consequence of the above discussion, the control law can be designed with the sole aim of tracking the reference rather than concerning about the stability in the Lyapunov sense of the overall system.

4. Converter Control

Due to parameters uncertainty and the switching nature of the considered system, sliding mode control techniques are the most suitable choice for converter control. In the following, the design of sliding mode control techniques for converter control will be described both for buck mode and boost mode.

4.1. Boost Mode

Let us initially consider the boost mode, that is $V_{net} \leq V_{bat}$. In this case, duty cycle $d_1 = 1$ and d_2 is active. This, in turn, implies that d_2 is selected as the control input u. Hence, the system equations can be written in the form of a bilinear system as:

$$\begin{aligned} \dot{x} &= \begin{bmatrix} -\left(\frac{1}{ESR_{net}} + \frac{1}{R_D}\right)\frac{1}{C_1} & -\frac{1}{C_1} & 0 \\ \frac{1}{L} & -\frac{R_L}{L} & 0 \\ 0 & 0 & -\frac{1}{ESR_{batt}C_2} \end{bmatrix} x + \begin{bmatrix} 0 & 0 & 0 \\ 0 & 0 & -\frac{1}{L} \\ 0 & \frac{1}{C_2} & 0 \end{bmatrix} xu + \begin{bmatrix} \frac{V_{net}}{ESR_{net}C_1} \\ 0 \\ \frac{V_{batt}}{ESR_{batt}C_2} \end{bmatrix} \\ &= (A + B_1)x + B_2 xu + \Gamma, \qquad u \in \{0,1\} \end{aligned} \tag{11}$$

The control objective, that is the regulation of $\iota_1(t)$ to a given reference $\bar{\iota}_1$, can be translated in the selection of the sliding function

$$\bar{\sigma}(t,x) = \bar{\iota}_1 - \iota_1(t,x) = \bar{\iota}_1 - \frac{V_{net}}{ESR_{net}} + x_1(t)\left(\frac{1}{ESR_{net}} + \frac{1}{R_D}\right). \tag{12}$$

Such selection of the sliding function implies that the relative degree of the system (11) with respect to $\bar{\sigma}$ (i.e. the minimum order r of the time derivative $\bar{\sigma}^{(r)}$ in which the control u explicitly appears) is equal to two. This, in turn, implies that a First Order Sliding Mode Control (FOSMC) is not effective to control the system dynamics. The adoption of Second Order Sliding Mode Control (SOSMC) techniques, instead, would guarantee robust performance to the controlled system at the cost of enforcing a discontinuous action on the control variable. Nevertheless, in the practical implementation of the control system, the input variable is fed to the PWM signal generator. Therefore, the control algorithm is required to generate a smooth signal (constrained in the compact interval $[0,1]$) to be sent to the PWM modulator (that will, in turn, generate a discontinuous signal in the set $\{0,1\}$). Hence, the control law that drives the PWM signal generator cannot be discontinuous. A possible solution is the reduction of the relative degree by selection of the sliding function as

$$\sigma(t,x) = \bar{\sigma}(t,x) + \frac{1}{\lambda}\dot{\bar{\sigma}}(t,x) \tag{13}$$

where λ is a positive definite design parameter. The selection of the sliding function as in (13) causes the relative degree between the system (11) and σ to be one. Hence, a SOSMC algorithm enforcing a chattering alleviation policy, which guarantees the smoothness of the input, can be employed.

In this work, a Suboptimal SOSMC will be designed in order to achieve the given control objective. Prior to the introduction of the Suboptimal SOSMC strategy, let us consider the following input transformation

$$v = u - \frac{1}{2}, \tag{14}$$

where provided $u \in [0,1]$, it holds that $v \in \mathcal{V} \coloneqq [-\frac{1}{2}, \frac{1}{2}]$. Considering the above input transformation, system (11) can be equivalently rewritten as

$$\dot{x} = \left(A + B_1 + \frac{1}{2}B_2\right)x + B_2 x v + \Gamma. \tag{15}$$

The input transformation (14) is required in order to reshape the asymmetric bound of the original input u in a symmetric bound of the new input v. Such symmetric bound of the new input allows for the implementation of control saturation necessary to constrain the duty cycle in the interval $[0,1]$ (see [29] for further details).

Let us consider the sliding function (13). Then, it is possible to derive an auxiliary system as follows:

$$\begin{cases} \xi_1(t,x) & = \sigma(t,x) \\ \dot{\xi}_1(t,x) & = \dot{\sigma}(t,x) = \dot{\tilde{\sigma}}(t,x) + \frac{1}{\lambda}\ddot{\tilde{\sigma}}(t,x) = \xi_2(t,x) \\ \dot{\xi}_2(t,x) & = \ddot{\xi}_1(t,x) = \ddot{\sigma}(t,x) = \dddot{\tilde{\sigma}}(t,x) + \frac{1}{\lambda}\ddddot{\tilde{\sigma}}(t,x) \end{cases} \tag{16}$$

Given the sliding function defined as in (12), the variable $\iota_1(t,x)$ as in (3), and the system dynamics represented as in (15), it is possible to derive the explicit form of the auxiliary system as

$$\begin{cases} \dot{\xi}_1 & = \xi_2 \\ \dot{\xi}_2 & = \varphi(x,v) + \gamma(x)w(t) \\ \dot{v} & = w \end{cases} \tag{17}$$

where $w(t)$ is the auxiliary control input to be designed to drive to zero the sliding function $\sigma(t,x)$ and

$$\varphi(x,v) \coloneqq \frac{1}{R_{Dnet}}\left\{\frac{1}{\lambda C_1 L}\left[R_L\dot{x}_2(t) - \dot{x}_1(t) + \left(\frac{1}{2} + v(t)\right)\dot{x}_3(t)\right] + \ddot{x}_1(t)\left(1 - \frac{1}{\lambda C_1 R_{Dnet}}\right)\right\}$$
$$\gamma(x) \coloneqq \frac{1}{\lambda C_1 R_{Dnet} L}x_3(t)$$

are uncertain bounded vector fields with $R_{Dnet} = \frac{R_D ESR_{net}}{R_D + ESR_{net}}$. In fact, provided that the ISS stability property holds for the open-loop system (hence, x is bounded in D), it is possible to find positive constants C, $\Gamma_{\min}$, and $\Gamma_{\max}$, such that

$$|\varphi(x,v)| \leq C \qquad \forall (x,v) \in \mathcal{D} \times \mathcal{V} \tag{18}$$
$$0 < \Gamma_{\min} \leq \gamma(x) \leq \Gamma_{\max} \qquad \forall x \in \mathcal{D}. \tag{19}$$

Note that condition $0 < X_3^- \leq x_3 \leq X_3^+$ allows for satisfaction of (19). Given the above discussion, the following theorem can be stated.

Theorem 3 (Control in boost mode). *Consider the system (11) and the auxiliary system (17) with uncertain dynamics bounded as in (18) and (19), where the variable v is define as in (14). Assume that the sequence of extremal values of $\sigma(t)$, say $\sigma_{t_k} = \sigma(t_k)$ (i.e., the value of σ at the last time instant at which $\dot{\sigma}(t) = 0$) is known. Define the auxiliary control input as*

$$w(t) = \begin{cases} -\alpha(t) K \operatorname{sgn}(\sigma - \eta\sigma_{t_k}) & \text{if } |v(t)| < \frac{1}{2} \\ -K \operatorname{sgn}(v(t)) & \text{if } |v(t)| \geq \frac{1}{2} \end{cases} \tag{20}$$

where $\eta \in [0.5, \bar{\eta}]$, with $\bar{\eta}$ being a positive parameter updated at each time instant t_s as $\bar{\eta} = \frac{\sigma_1(t_s)}{\sigma_{t_k}}$ with t_s being, such that $|v(t_s)| \geq \frac{1}{2}$. Moreover,

$$\alpha(t) = \begin{cases} 1, & \text{if } (\sigma(t) - \eta\sigma_{t_k})(\sigma_{t_k} - \sigma(t)) < 0 \\ \alpha^*, & \text{if } (\sigma(t) - \eta\sigma_{t_k})(\sigma_{t_k} - \sigma(t)) \geq 0 \end{cases} \tag{21}$$

with α^* and K being positive parameters selected as follows:

$$\begin{cases} \alpha^* \in [0,1) \cap \left(0, \frac{3\Gamma_{\min}}{\Gamma_{\max}}\right) \\ K > \frac{C}{\Gamma_{\min}} \end{cases}. \tag{22}$$

Then, it holds that the converter input current is, such that

$$\lim_{t\to\infty} \iota_1(t) = \bar{\iota}_1, \tag{23}$$

while the control input u is smooth and constrained in the interval $[0,1]$. Moreover, the zero dynamics are stable.

Proof. Firstly, system (15), which is equivalent to system (11), has relative degree equal to one with respect to the sliding function (13). This allows for augmenting the system order to implement a chattering alleviation strategy as performed in (17). Proof of finite time convergence of the auxiliary system (17) to the origin of the state plane (ξ_1, ξ_2) follows directly from [33]. This, in turn, implies that there exists a finite time T, such that

$$\sigma(t) = \xi_1(t) \equiv 0 \quad \forall t \geq T.$$

As a consequence, from (13), it holds that for all $t \geq T$

$$\dot{\bar{\sigma}} = -\lambda\bar{\sigma},$$

which guarantees that $\bar{\sigma}$ tends to zero exponentially and as a consequence the exponential convergence of the variable $\iota_1(t,x)$ towards the reference $\bar{\iota}_1$. Once on the manifold, the stability of the zero dynamics is guaranteed by the ISS property proved in Theorem 2. Finally, as detailed in [29], the overall control input

$$u = \frac{1}{2} + w(0) + \int_0^t w(\tau)\mathrm{d}\tau,$$

with $w(t)$ selected as in (20) guaranteeing that the auxiliary variable $v(t) \in \mathcal{V}$ for all $t \geq 0$, and, as a consequence, $u(t) \in [0,1]$ for all $t \geq 0$. □

4.2. Buck Mode

Buck mode occurs when $V_{net} > V_{bat}$. In this case, the duty cycle d_1 is kept active while $d_2 = 1$, which implies that system (2) can be rewritten as

$$\dot{x} = (A + B_2)x + B_1 xu + \Gamma, \qquad u \in \{0, 1\} \tag{24}$$

where $u = d_1$. Similar to the above analysis, let us consider the input transformation (14), which allows for the equivalent reformulation of system (24) as

$$\dot{x} = \left(A + B_2 + \frac{1}{2}B_1\right)x + B_1 xv + \Gamma, \qquad v \in \left\{-\frac{1}{2}, \frac{1}{2}\right\} \tag{25}$$

with the new control input v being bounded in a symmetric set. Differently from the boost case, in buck mode selection of the sliding function

$$\sigma(t, x) = \bar{\sigma}(t, x), \tag{26}$$

with $\bar{\sigma}$ defined as in (12), is sufficient to achieve a relative degree of system (24) equal to one. Thus, let us consider the sliding function (26) and the associated auxiliary system

$$\begin{cases} \dot{\xi}_1 &= \dot{\sigma} = \xi_2 \\ \dot{\xi}_2 &= \ddot{\sigma} = \varphi(x, v) + \gamma(x)w(t) \\ \dot{v} &= w \end{cases} \tag{27}$$

where

$$\varphi(x, v) := \frac{1}{C_1 R_{Dnet}}\left[-\frac{\dot{x}_1(t)}{R_{Dnet}} - \left(\frac{1}{2} + v(t)\right)\dot{x}_2(t)\right], \tag{28}$$

$$\gamma(x) := -\frac{1}{C_1 R_{Dnet}}x_2(t). \tag{29}$$

Note that the state variable x_2 denotes the inductor current, which can take both positive and negative values. Therefore, differently from the buck case, it is not possible to bound the uncertain vector field $\gamma(x)$, such that condition (19) holds, which prevents direct application of any SMC control technique. A possible solution to overcome this obstacle resides in the definition of a two-stage control strategy. Such a strategy consists of defining a nonlinear controller able to operate throughout the entire state space but only use it to operate in a relatively small subset of that space and use a linear controller when the system state lies inside such a set.

Preliminarily, let us define the following sets

$$\Omega_1 := \{x \in \mathcal{D} \colon |x_2| \geq \hat{\imath}_L\}, \tag{30}$$

$$\Omega_2 := \{x \in \mathcal{D} \colon |x_2| < \hat{\imath}_L\} = \mathcal{D} \backslash \Omega_1, \tag{31}$$

where $\hat{\imath}_L$ is a positive constant to be designed. The two-stage control algorithm proposed in this paper for converter control in buck mode is structured as follow (see Figure 2):

1. Adoption of a monotonic SOSMC when $x \in \Omega_1$,
2. Adoption of a monotonic linear control law to be activated when $x \in \Omega_2$.

The idea behind this approach is to adopt a monotonic SOSMC as long as x_2 is not too close to zero to keep the $\gamma(x)$ term in (29) different from zero and to allow (19) to hold in Ω_1. If the variable x_2 is required to cross the zero value, then a linear control law (designed and tuned after linearization of system (24)) can be adopted. Finally, when x_2 is sufficiently far from zero, the SOSMC algorithm can be enforced again. Note that currents x_2 and $\imath_1$ have similar average dynamics. If the average value of x_2 is increasing (decreasing), then

the average of ι_1 will also increase (decrease). Therefore, the custom control law that allows x_2 to cross the zero value will also allow ι_1 to cross zero (as depicted in Figure 2).

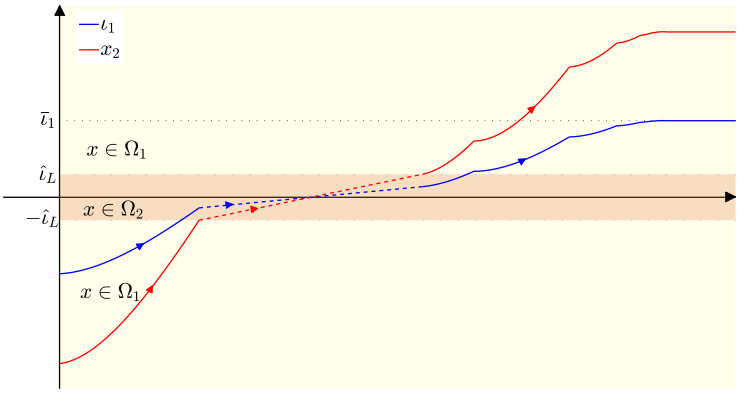

Figure 2. Transition between monotonic Suboptimal SOSMC (37) (**solid line**) and control law (38) (**dashed line**).

Therefore, as long as $x \in \Omega_1$, conditions (18) and (19) are satisfied. As it will be detailed later, monotonicity of both control laws is a crucial characteristic for their combined adoption.

It is now possible to introduce the *monotonic* Suboptimal SOSMC algorithm presented in [25]. Consider the auxiliary system (27) and the auxiliary control input defined as

$$w(t) = \begin{cases} -\alpha(t) K \operatorname{sgn}(\sigma - \eta\sigma_{t_k}) & \text{if } |v(t)| < \frac{1}{2} \\ -K \operatorname{sgn}(v(t)) & \text{if } |v(t)| \geq \frac{1}{2} \end{cases} \tag{32}$$

with

$$\alpha(t) = \begin{cases} 1, & \text{if } (\sigma(t) - \eta\sigma_{t_k})\sigma_{t_k} \geq 0 \\ \alpha^*, & \text{if } (\sigma(t) - \eta\sigma_{t_k})\sigma_{t_k} < 0 \end{cases} \tag{33}$$

$$\eta \in [0; 1). \tag{34}$$

As detailed in [25], the requirement of monotonic convergence to zero of the sliding variable may be fulfilled by designing the parameters α^* and K to be selected as

$$\alpha^* \in [1; +\infty) \cap \left[\frac{C + (1-\eta)\Gamma_{\max} K}{\eta \Gamma_{\min} K}; +\infty \right), \tag{35}$$

$$K > \frac{C}{\Gamma_{\min}}. \tag{36}$$

The above algorithm can be adopted when $x \in \Omega_1$. When the state trajectory belongs to Ω_2, condition (19) cannot be met and an alternative control law must be defined. In principle, any nonlinear control law able to control the system trajectories within Ω_2 or to steer them outside Ω_2 could be adopted. Nevertheless, since the set Ω_2 can be designed to be rather small, linear control laws based on the linearization of system (24) can also be taken into account since they preserve their stability properties in a neighbor of the point around which linearization is performed.

The above arguments on the two-stage controller can be summarized in the following theorem.

Theorem 4 (Control in buck mode). *Consider system (24), the sliding function defined in (26), and the auxiliary system (27), with uncertain dynamics defined as in (28)–(29), where the variable v is defined as in (14). Consider regions Ω_1 and Ω_2 defined in (30)–(31), and the two-stage control law defined as*

$$v = \begin{cases} w(\sigma(t_s)) + \int_{t_s}^{t} w(\sigma(\tau))\mathrm{d}\tau, & \text{if } x \in \Omega_1 \quad (37) \\ k_P\sigma(t) + k_I \int_{t_s}^{t} \sigma(\tau)\mathrm{d}\tau - \frac{1}{2}, & \text{if } x \in \Omega_2 \quad (38) \end{cases}$$

where w is designed as in (32), with t_s being such that $x(t_s^-) \in \Omega_2$ and $x(t_s^+) \in \Omega_1$. Parameters $\alpha(t)$, η α^*, and K selected as in (33)–(36), respectively, and where $\sigma_{t_k} = \sigma(t_k)$ indicates the sequence of extremal values of $\sigma(t)$ assumed to be known. Parameters k_P and k_I are chosen so that monotonic motion of the state trajectories when $x \in \Omega_2$ is guaranteed. Then, there exists positive T, such that

$$\sigma(t, x) \equiv 0 \;\; \forall t \geq T, x \in \mathcal{D}, \tag{39}$$

while producing a smooth control input u constrained in the interval $[0, 1]$. Moreover, the zero dynamics are stable.

Proof. System (24) can be equivalently reformulated as system (25) with v being defined as in (14). System (25) has relative degree one with respect to the sliding function (26). This allows for augmenting the system order to implement a chattering alleviation strategy by definition of the auxiliary system (27) controlled by the auxiliary input w.

Let us assume that initially $x_0 = [x_{10}, x_{20}, x_{30}]^\top \in \Omega_1$. Three cases can arise: either the desired equilibrium point $\bar{x}$ is, such that $\bar{x} \in \Omega_1$ and no crossing of Ω_2 is required; $\bar{x} \in \Omega_1$ and crossing of Ω_2 is required; or $\bar{x} \in \Omega_2$. In the first case, monotonic finite time convergence of the auxiliary system to the origin of the state plane (ξ_1, ξ_2) follows directly from [25]. Such monotonic motion of $\sigma(t)$ translates in monotonicity of $\iota_1(t)$ and $x_2(t)$, which, in turn, guarantees that even during transit the state $x(t)$ will not enter the set Ω_2. This, in turn, implies that there exists a finite time T, such that

$$\sigma(t) = \xi_1(t) \equiv 0 \quad \forall t \geq T.$$

Let us now consider the case when $x_0 \in \Omega_1$ and $\bar{x} \in \Omega_1$, but crossing is required. In this case, three phases can be identified:

1. $x_0 \in \Omega_1$ and $\mathrm{sgn}(x_{20}) = -\mathrm{sgn}(\bar{\iota}_1)$: the SOSMC law (37) is applied to the system, and it monotonically drives $\iota_1(t)$ (and $x_2(t)$) towards the boundary of Ω_1;
2. $x(t) \in \Omega_2$: on the boundary between Ω_1 and Ω_2 ,the control law switches to (38), and $x_2(t)$ is monotonically increased (or decreased, depending on the sign of $\bar{\iota}_1$) until the state exits the set Ω_2;
3. $x(t) \in \Omega_1$: the SOSMC law (37) is again applied to the system, and it monotonically (and in finite time) drives $\iota_1(t)$ towards $\bar{\iota}_1$.

While monotonicity while in Ω_1 is guaranteed by the selection of the control law (37), monotonicity while in Ω_2 can be easily guaranteed by appropriately tuning the PI gains k_P and k_I so that no oscillations nor overshoot is generated. Monotonicity of both control laws allows for avoiding chattering on the boundary of the two regions.

Finally, in the case where $x_0 \in \Omega_1$ and $\bar{x} \in \Omega_2$, only the first two steps above will be operated, thus still guaranteeing monotonic convergence towards the desired equilibrium point

In the case where $x_0 = [x_{10}, x_{20}, x_{30}]^\top \in \Omega_2$ and $\bar{x} \in \Omega_1$, then the same reasoning presented in Steps 2 and 3 hold for the proposed control law. Finally, once the system trajectory reaches the manifold, stability of the residual dynamics is ensured by the ISS property of the system. □

Remark 2 (Uniting Control). *The switching control strategy proposed in Theorem 4 draws inspiration from the uniting control techniques presented in ([27], Chapter 4) which is based on the adoption of two controllers to globally stabilize the desired equilibrium point. The first controller is designed to guaranteed global convergence to a neighborhood of the desired equilibrium, while the second control should guarantee local asymptotic stability of the desired equilibrium. This approach allows using a SOSMC as a globally stabilizing controller and a simple proportional–integral controller as a locally stabilizing controller. As for the PI controller, its gains can be easily tuned based on the linearization of system (24).*

Remark 3 (Exponential and Finite Time Convergence). *It is worth underscoring a fundamental difference between the result presented in Theorems 3 and 4. Due to order augmentation of the sliding function (13), only exponential convergence of the current ι_1 towards its reference $\bar{\iota}_1$ can be obtained in case of boost mode. In case of buck mode, instead, Theorem 4 proves finite time convergence of the current ι_1 towards its reference $\bar{\iota}_1$. A possible solution to speed up the exponential convergence in the case of buck mode is to increase the value of λ in (13).*

4.3. Supervisory Control

In view of what has been expressed above, it is clear that the entire buck–boost converter controller is not a unique algorithm. Indeed, during boost mode, the active controller is the SOSM control algorithm described in Theorem 3, while for current control in buck mode, a two-stage control algorithm has been designed. If the state trajectory belongs to the set Ω_1 indicated in (30), then the monotonic SOSM control algorithm presented in (37) is adopted, while if the state trajectory belongs to the set Ω_2 indicated in (31), then the feedback-based monotonic control algorithm (38) is adopted. This recalls the need for a higher-level controller, i.e., a supervisory controller, responsible for the selection of the required controller according to the value of the converter state. Such a supervisor can be constructed as a finite-state machine presented in Figure 3.

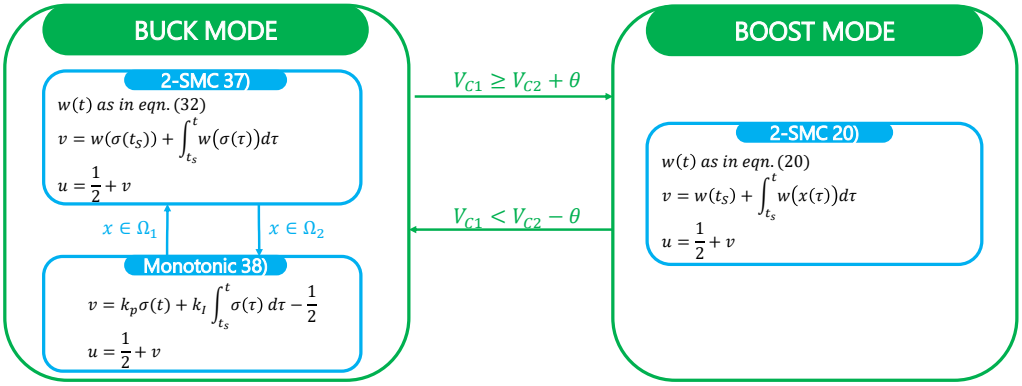

Figure 3. Supervisory controller.

Despite Theorems 3 and 4 proving the stability of the respective closed-loop systems, switching among the three controllers may generate two undesired effects: instability and chattering. Indeed, as proved in [34], switching between stable system does not guarantee that the switched system is stable. In the present case, switching among the different controllers implies a variation of the active control law u. Nevertheless, Theorem 2 proves that the system cannot undergo instability for any arbitrarily chosen control law u. Hence, instability can be discarded. The chattering phenomenon consists of the fast switching between active controllers. With reference to the switches among controller (37) and (38), as explained in Theorem 4, monotonicity of both controllers guarantees the absence of chattering. Finally, in order to avoid chattering when switching from buck to boost mode and vice versa, hysteresis band θ can be adopted.

5. Simulation Results

The proposed control algorithm for current control of a buck–boost converter and the associated supervisory strategy were tested in a detailed MATLAB/Simulink/SimPowerSystem simulator, shown in Figure 4, and it is composed of six blocks:

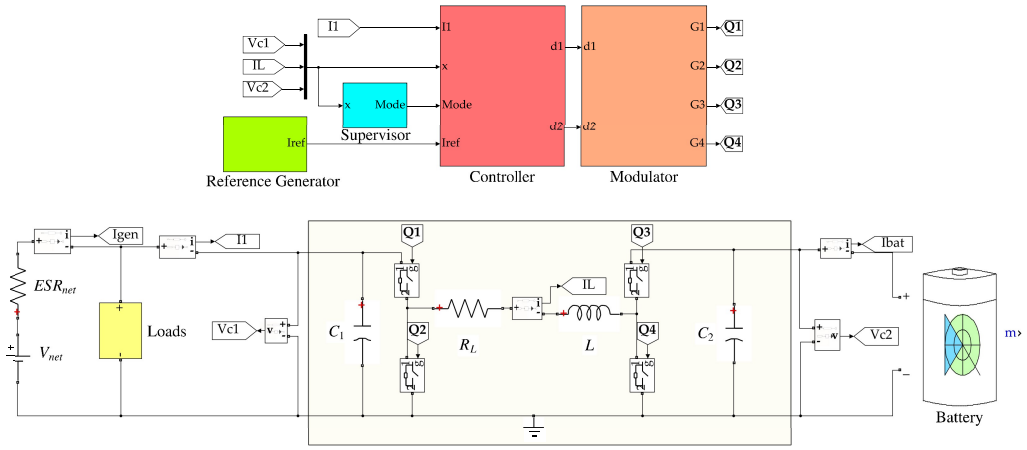

Figure 4. MATLAB/Simulink/SimPowerSystem simulation model.

- Supervisor: implements the supervisory finite-state machine designed according to Figure 3.
- Controller: implements the control algorithms presented in Theorems 3 and 4.
- Modulator: realizes the PWM switching modulation for switches G_1, G_2, G_3, and G_4.
- Reference Generator: this block selects the proper reference converter input current $\bar{\imath}_1$ to be tracked by the active controller.
- Loads: this block contains a set of resistors which can be activated or deactivated during the operating time.
- Battery: this is the implementation of an accurate battery model [35].

The converter and network parameters are shown in Table 1.

Table 1. Converter and network parameters.

Parameter	Value	
ESR_{net}	70	[mΩ]
ESR_{batt}	30	[mΩ]
R_L	10	[mΩ]
C_1	2.2	[mF]
C_2	16	[μF]
L	23	[mH]
f	40	[kHz]
$\bar{\imath}_{gen}$	16	[A]

Specifically, $V_{NET} = 540\,\mathrm{V}$ indicates the nominal value of the aeronautic generator voltage connected to the main bus, while $V_{BAT} = 400\,\mathrm{V}$ indicates the nominal value of the battery voltage. The switching frequency of the PWM generator is indicated here with f. In nominal conditions, i.e., when both generator and battery operate with nominal voltage, the converter acts as a buck converter, thus control laws (37) and (38) are adopted. However, there may be some cases when the bus voltage becomes smaller than the battery voltage. For instance, this may occur in case of a generator operating with reduced capabilities, or in the case of over-voltage of the battery. In such scenarios, the converter will perform as a boost converter. In both buck and boost mode, the control goal is to control the

input converter current ι_1 to a given reference value, despite sudden load variations and parameter uncertainty. The reference value of the ι_1 current is provided by the reference generator block. Typically, in the framework of the MEA, the reference generator block is implemented as an external higher-level supervisor responsible for selecting the adequate operating set points for each electrical subsystem. A possible logic behind the selection of the current reference is the following:

- If the generator current is below a threshold value (indicated with $\bar{\iota}_{gen}$ in Table 1), the objective is to control the converter input current to a prescribed positive value in order to charge the battery.
- Otherwise, if the bus current overcomes such a threshold value, the objective is to drive the bus current to the threshold value. In this case, the battery current is either lowered or reversed so that the battery will help the aeronautic generator feeding the connected loads.

Nevertheless, the detailed analysis of such high-level logic is not within the scope of this work, and further details can be found in [36].

In what follows, two simulation scenarios are presented in order to show the effectiveness of the proposed control architecture and its reference-tracking capabilities both in boost and in buck mode.

5.1. Simulation Results in Boost Mode

Boost mode is activated when $V_{NET} < V_{BAT}$. In this case, the generator and the battery voltage values were set to 300 V and 450 V, respectively, and the controller (20) was selected. The numerical values of the control parameters for these algorithms are presented in Table 2.

Table 2. Network parameters and load variation in boost mode.

(**a**) Controller Parameters	
Parameter	**Value**
K	1
α^*	5
η	0.33

(**b**) Load Resistance and Current Reference variation		
Load Resistance	**Current Reference**	**Interval**
60Ω	4 A	[0, 5] s
7.5Ω	−23.15 A	[5, 10] s
30Ω	4 A	[10, 15] s
10Ω	−13.50 A	[15, 20] s
20Ω	1.12 A	[20, 25] s
15Ω	−3.8 A	[25, 30] s

In the designed simulation test, the power grid undergoes sudden load variations indicated in Table 2b. During the first 5 s of simulation, the reference current is set to 4 A, thus the battery is being charged, and as shown in Figure 5, such reference is tracked with good performance in terms of transient time. During this time interval, the generator feeds both the battery and the connected loads, and its current is equal to 9 A. At 5 s the resistance of the total connected loads suddenly changes to 7.5Ω, as reported in Table 2b, the generator current increases above its current threshold $\bar{\iota}_{gen}$, and a new value of $\bar{\iota}_1$ is provided. In this case, the battery current is negative, meaning that the battery is supporting the generator to feed the loads. The rest of the simulation test proceeds with the same rationale: a current reference $\bar{\iota}_1$ is provided according to the connected load and the control algorithm in (20) successfully tracks the reference with good performance. The active duty

cycle d_2, the generator side, and the battery side voltages are shown in Figure 6, while Figure 7 shows the evolution of the sliding function in (12).

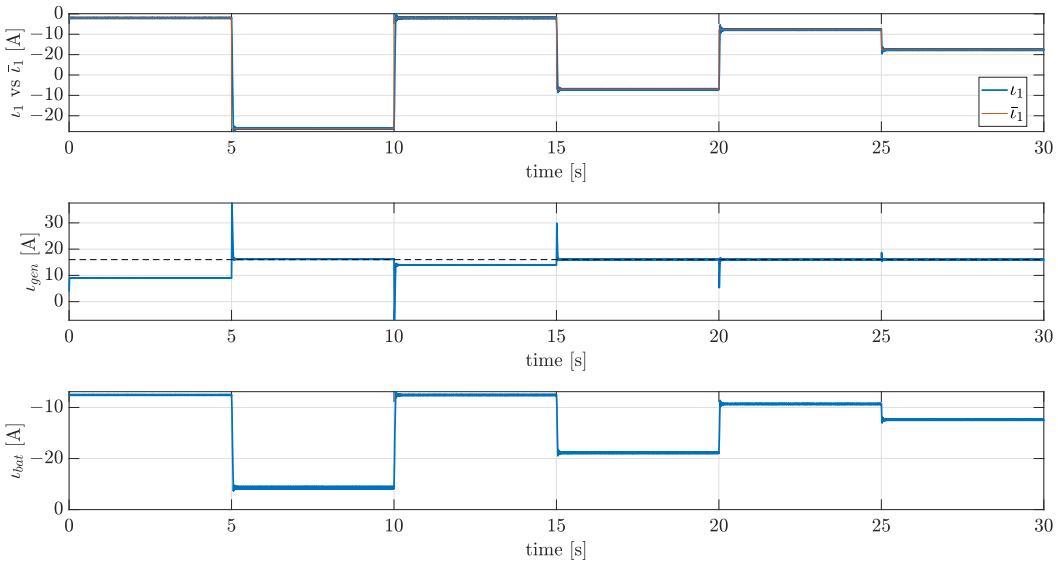

Figure 5. Boost mode. From top to bottom: converter input current ι_1 (**blue solid line**) and current reference $\bar{\iota}_1$ (**red solid line**); generator current ι_{gen} (**blue solid line**) and its threshold value (**black dashed line**); battery current ι_{batt} (**blue solid line**).

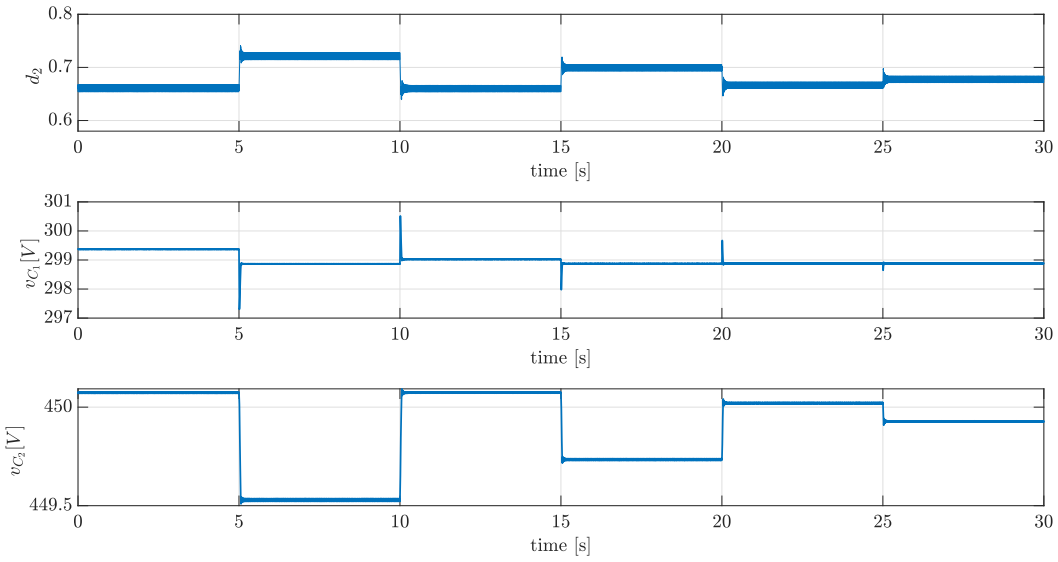

Figure 6. Boost mode. From top to bottom: active duty cycle d_2; generator side voltage v_{C_1}; battery side voltage v_{C_2}.

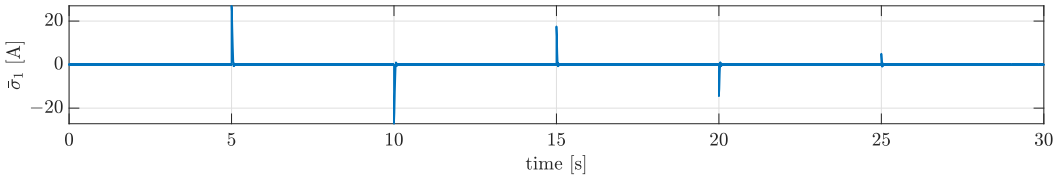

Figure 7. Boost mode. Sliding variable $\bar{\sigma}_1$ in (12).

5.2. Simulation Results in Buck Mode

Buck mode is activated when $V_{NET} \geq V_{BAT}$. In this case, the generator and the battery voltage values were set to 540 V and 300 V, respectively, and the controller (37) and (38) is selected. Specifically, as detailed in Theorem (4), the control law (37) is chosen when $x \in \Omega_1$, while control (38) is chosen when $x \in \Omega_2$. The numerical values of the control parameters for these algorithms are presented in Table 3a.

Table 3. Network parameters and load variation in buck mode.

(**a**) Controller Parameters

Parameter	**Value**
K	0.1
α^*	5
η	0.33
$\hat{\imath}_L$	3

(**b**) Load Resistance and Current Reference variation

Load Resistance	**Current Reference**	**Interval**
80Ω	4 A	[0, 5] s
60Ω	4 A	[5, 10] s
20Ω	−16.25 A	[10, 15] s
30Ω	−5.75 A	[15, 20] s
60Ω	4 A	[20, 25]s
80Ω	4 A	[25, 30] s

Similar to the case of Boost mode, in the proposed scenario for Buck mode, sudden variations for the total connected loads and the converter reference current occur. Initially, the resistance of the total connected loads equals 80Ω, and the current reference is set to 4 A. As evident from the upper plot in Figure 8, the control algorithm manages to drive the converter current to the given reference. The plot in the center of Figure 8 shows that the generator current is below the threshold value of 16 A, while the battery is charging with a current approximately equal to 9.5 A. After 5 s, the total resistance of the connected loads changes to 60Ω, while the converter reference current remains equal to 4 A. In this case, the control algorithm proves its robustness against sudden load variations. Indeed, the two-stage controller manages to almost immediately steer the converter current to 4 A. As can be appreciated in the middle plot of Figure 8, the generator current increases to a value approximately equal to 15 A, still below the generator current.

At time $t = 10$ s, the total resistance of the connected loads is 20Ω. In this case, the generator current spikes to a value above the generator threshold. As shown by Table 3b, the converter reference current is switched to −16.25 A. The selected reference value guarantees that the generator current is driven to the threshold value within one second. In this case, as evident from the bottom plot of Figure 8, the battery current is negative, thus implying that the battery is now supporting the main generator in feeding the loads.

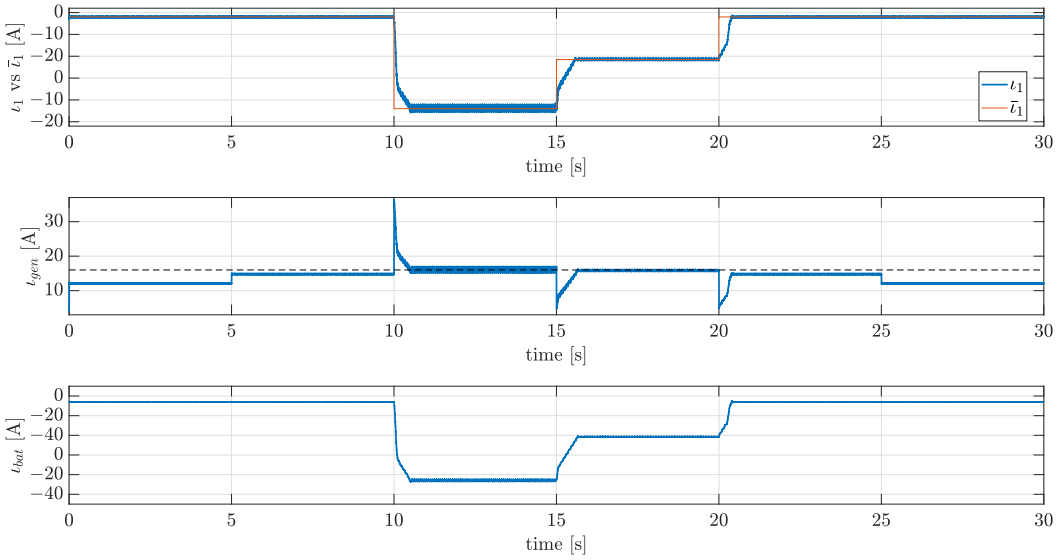

Figure 8. Buck mode. From top to bottom: converter input current ι_1 (**blue solid line**) and current reference $\bar{\iota}_1$ (**red solid line**); generator current ι_{gen} (**blue solid line**) and its threshold value (**black dashed line**); battery current ι_{batt} (**blue solid line**).

At time $t = 15$ s, the total resistance of the connected loads is 30 Ω, while the converter reference current is set to -5.75 A. Similar to the previous case, the converter input current is driven to the desired reference in a monotonic way, and the generator current is set to its threshold value. The battery current is still negative but with a smaller magnitude.

The total resistance of the connected loads becomes equal to 60 Ω at $t = 20$ s; this allows for selection of a positive reference value for the converter input current equal to 4 A. As in the interval $[5, 10]$ s, the generator current reaches an approximate value of 15 A, and the converter input current reaches the given reference. It is interesting to notice how, as stated in the theoretical analysis, the current ι_1 monotonically converges towards the reference both when $x \in \Omega_1$ and $x \in \Omega_2$ (see also Figure 9).

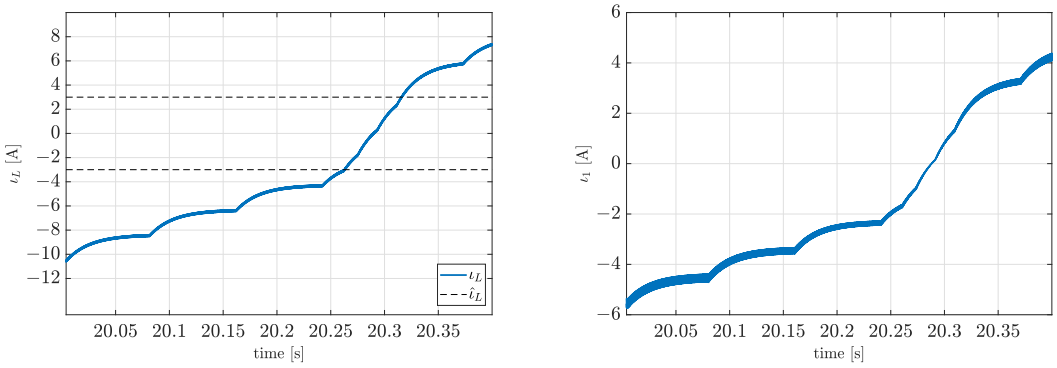

Figure 9. Buck mode. Monotonic convergence of current ι_L (**blue solid line**) compared with threshold $\hat{\iota}_L$ (**black dashed line**), left plot; monotonic convergence of of current ι_1 (**blue solid line**), right plot.

Finally, at $t = 25$ s, the load resistance is set equal to 80Ω, while no variation in the converter input current reference occurs, thus resorting the initial configuration of the network. The active duty cycle d_1, the generator side, and the battery side voltages are shown in Figure 10, while Figure 11 shows the evolution of the sliding function in (12).

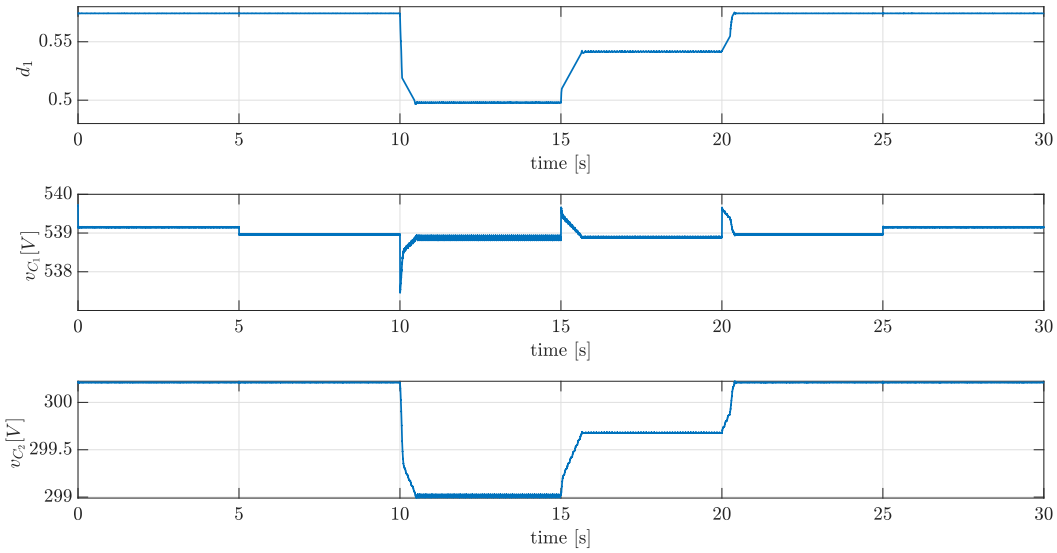

Figure 10. Buck mode. From top to bottom: active duty cycle d_1; generator side voltage v_{C_1}; battery side voltage v_{C_2}.

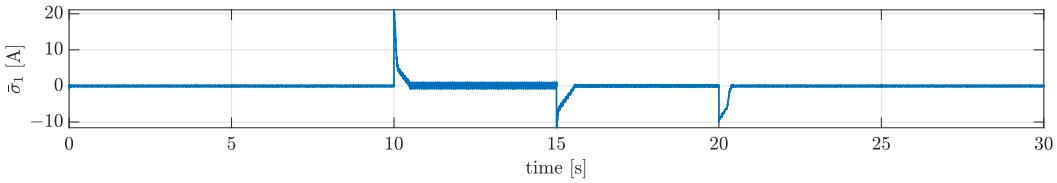

Figure 11. Buck mode. Sliding variable $\bar{\sigma}_1$ in (12)

6. Conclusions

This paper presented the theoretical stability analysis and control of a buck–boost converter based on SOSM and uniting control for an MEA application. Specifically, a bidirectional converter was used to regulate the power flow between the power generator and a battery in order to limit the aircraft generator current. Stability of the converter in the Lyapunov sense was proved, resorting to the notion of ISS. Furthermore, the design of a switching control law consisting of a (monotonic) Saturated Suboptimal Second Order Sliding Mode Control and a feedback based monotonic control algorithm was presented. While convergence of the closed-loop system can be achieved using the sole sliding mode control law in boost mode, it was demonstrated why a switching control law is necessary in buck mode to overcome the difficulties generated by the nonlinear input gain function of the system not being sign definite . Finally, a simulation campaign was presented to emulate the scenario of current control in an MEA application. This simulation campaign confirms the effectiveness and correctness of the designed control law, both in buck and in boost mode. As future research, the comparison of the results obtained in this work with several different power converters used for the same purpose is of high interest since not many converters have been investigated for applications related to MEA. Moreover, further research will move towards the definition of distributed control laws to orchestrate multiple converters throughout the aircraft power grid.

Author Contributions: Conceptualization, A.R. and A.C.; methodology, A.R.; software, A.R.; validation, A.R. and A.C.; formal analysis, A.R.; investigation, A.R.; resources, A.C.; data curation, A.R.; writing—original draft preparation, A.R.; writing—review and editing, A.C.; visualization, A.R.; supervision, A.C.; project administration, A.C.; funding acquisition, A.C. All authors have read and agreed to the published version of the manuscript.

Funding: This work was supported by the CleanSky2 grant Programme: H2020-CS2-CFP10-2019-01 JTI-CS2-2019-CfP10-SYS-02-59 Proposal: 886559 HYPNOTIC.

Data Availability Statement: No data reported.

Conflicts of Interest: The authors declare no conflict of interest.

List of Symbols

Symbol	Definition
v_{C_1}, v_{C_2}	Voltage measurement at input and output of the converter
v_L	Inductor voltage
ι_{gen}, ι_{batt}	Generator and battery current measurement
ι_1	Converter input current measurement
ι_L	Inductor current
Q_1, Q_2, Q_3, Q_4	Converter switches
d_1, d_2	Duty cycles of the two converter legs
V_{net}, V_{batt}	Generator and battery voltage
ESR_{net}, ESR_{batt}	Generator and battery inner resistance
R_L	Inductor resistance
R_D	Total connected loads
C_1, C_2	Converter input and output capacitor
L	Converter inductor
f	Switching frequency
$\bar{\iota}_{gen}$	Generator current setpoint
σ	Sliding function variable
w	Auxiliary control variable
α, K, η	SubOptimal Second Order SMC gains

References

1. More Electric Aircraft. Available online: www.moreelectricaircraft.com (accessed on 15 January 2023).
2. POA. POA-Power Optimised Aircraft Project. 2002–2005. Available online: http://www.2020-horizon.com/POA-Power-optimised-aircraft(POA)-s16028.html (accessed on 15 January 2023).
3. Clean Aviation Website. 2022. Available online: https://www.clean-aviation.eu/ (accessed on 15 January 2023).
4. Hyundai Plans to Put You in a Flying Taxi in Just 8 Years. Available online: https://www.cnet.com/roadshow/news/hyundai-flying-taxi-urban-air-mobility/ (accessed on 25 August 2021).
5. Ismagilov, F.; Varyukhin, A.; Vavilov, V.; Bekuzin, V.; Gusakov, D. Electric Machines Development Process for Aviation Hybrid Propulsion Systems. In Proceedings of the IECON 2020 the 46th Annual Conference of the IEEE Industrial Electronics Society, Singapore, 18–21 October 2020; pp. 955–960.
6. Wheeler, P.; Bozhko, S. The More Electric Aircraft: Technology and challenges. *IEEE Electrif. Mag.* **2014**, *2*, 6–12. [CrossRef]
7. Lang, X.; Yang, T.; Huang, Z.; Wang, Z.; Bozhko, S.; Wheeler, P. Instantaneous Power Control Within an Advanced Power Generation Center for More-Electric Aircraft Applications. *IEEE Trans. Transp. Electrif.* **2022**, *8*, 3261–3274. [CrossRef]
8. Tariq, M.; Maswood, A.I.; Gajanayake, C.J.; Gupta, A.K. Aircraft batteries: Current trend towards more electric aircraft. *IET Electr. Syst. Transp.* **2017**, *7*, 93–103. [CrossRef]
9. Mohamed, M.A.A.; Yeoh, S.; Atkin, J.; Khalaf, M.; Bozhko, S. Analysis and Design of Battery Controller for More Electric Aircraft Application. In Proceedings of the 2021 IEEE International Power and Renewable Energy Conference (IPRECON), Kollam, India, 24–26 September 2021; pp. 1–6.
10. Cavallo, A.; Russo, A.; Canciello, G. Control of Supercapacitors for smooth EMA Operations in Aeronautical Applications. In Proceedings of the 2019 American Control Conference (ACC), Philadelphia, PA, USA, 10–12 July 2019; pp. 4948–4954.
11. Russo, A.; Cavallo, A. Supercapacitor stability and control for More Electric Aircraft application. In Proceedings of the 2020 European Control Conference (ECC), St. Petersburg, Russia, 12–15 May 2020; pp. 1909–1914.
12. Chan, C.Y. Adaptive Sliding-Mode Control of a Novel Buck-Boost Converter Based on Zeta Converter. *IEEE Trans. Circuits Syst. II Express Briefs* **2022**, *69*, 1307–1311. [CrossRef]
13. Li, X.; Liu, Y.; Xue, Y. Four-Switch Buck–Boost Converter Based on Model Predictive Control With Smooth Mode Transition Capability. *IEEE Trans. Ind. Electron.* **2021**, *68*, 9058–9069. [CrossRef]
14. Waffler, S.; Kolar, J.W. A Novel Low-Loss Modulation Strategy for High-Power Bidirectional Buck + Boost Converters. *IEEE Trans. Power Electron.* **2009**, *24*, 1589–1599. [CrossRef]
15. Ray, B.; Romney-Diaz, A. Constant frequency resonant topologies for bidirectional DC/DC power conversion. In Proceedings of the IEEE Power Electronics Specialist Conference—PESC '93, Seattle, WA, USA, 20–24 June 1993; pp. 1031–1037.
16. Schupbach, R.; Balda, J. Comparing DC-DC converters for power management in hybrid electric vehicles. In Proceedings of the IEEE International Electric Machines and Drives Conference, 2003. IEMDC'03, Madison, WI, USA, 1–4 June 2003; Volume 3, pp. 1369–1374.

17. Kim, C.E.; Han, S.K.; Yi, K.H.; Lee, W.J.; Moon, G.W. A New High Efficiency ZVZCS Bi-directional DC/DC Converter for 42V Power System of HEVs. In Proceedings of the 2005 IEEE 36th Power Electronics Specialists Conference, Dresden, Germany, 16 June 2005; pp. 792–797.
18. AL-Nussairi, M.K.; Bayindir, R.; Padmanaban, S.; Mihet-Popa, L.; Siano, P. Constant Power Loads (CPL) with Microgrids: Problem Definition, Stability Analysis and Compensation Techniques. *Energies* **2017**, *10*, 1656. [CrossRef]
19. Singh, S.; Gautam, A.R.; Fulwani, D. Constant power loads and their effects in DC distributed power systems: A review. *Renew. Sustain. Energy Rev.* **2017**, *72*, 407–421. [CrossRef]
20. Martinez-Trevino, B.A.; Jammes, R.; Aroudi, A.E.; Martinez-Salamero, L. Sliding-mode control of a boost converter supplying a constant power load. *IFAC-PapersOnLine* **2017**, *50*, 7807–7812. [CrossRef]
21. Cavallo, A.; Canciello, G.; Russo, A. Buck-Boost Converter Control for Constant Power Loads in Aeronautical Applications. In Proceedings of the 2018 IEEE Conference on Decision and Control (CDC), Miami, FL, USA, 17–19 December 2018; pp. 6741–6747.
22. Canciello, G.; Russo, A.; Guida, B.; Cavallo, A. Supervisory Control for Energy Storage System Onboard Aircraft. In Proceedings of the 2018 IEEE International Conference on Environment and Electrical Engineering and 2018 IEEE Industrial and Commercial Power Systems Europe (EEEIC/I CPS Europe), Palermo, Italy, 12–15 June 2018; pp. 1–6.
23. Cavallo, A.; Canciello, G.; Russo, A. Supervised Energy Management in Advanced Aircraft Applications. In Proceedings of the 2018 European Control Conference (ECC), Limassol, Cyprus, 12–15 June 2018; pp. 2769–2774.
24. Sontag, E.; Wang, Y. New characterizations of Input to State Stability. *IEEE Trans. Autom. Control.* **1996**, *41*, 1283–1294. [CrossRef]
25. Bartolini, G.; Pisano, A.; Punta, E.; Usai, E. A Survey of Applications of Second-order Sliding Mode Control to Mechanical Systems. *Int. J. Control.* **2003**, *76*, 875–892. [CrossRef]
26. Ferrara, A.; Incremona, G.P.; Cucuzzella, M. *Advanced and Optimization Based Sliding Mode Control: Theory and Applications*; Society for Industrial and Applied Mathematics: Philadelphia, PA, USA, 2019.
27. Sanfelice, R.G. *Hybrid Feedback Control*; Princeton University Press: Princeton, NJ, USA, 2021.
28. Akhtar, A.; Sanfelice, R.G. A Class of Hybrid Geometric Controllers for Robust Global Asymptotic Stabilization on S^1. In Proceedings of the 2022 American Control Conference (ACC), Atlanta, GA, USA, 8–10 June 2022; pp. 874–879.
29. Ferrara, A.; Rubagotti, M. A Sub-Optimal Second Order Sliding Mode Controller for Systems With Saturating Actuators. *IEEE Trans. Autom. Control.* **2009**, *54*, 1082–1087. [CrossRef]
30. Ahmed, M.R.; Todd, R.; Forsyth, A.J. Predicting SiC MOSFET Behavior Under Hard-Switching, Soft-Switching, and False Turn-On Conditions. *IEEE Trans. Ind. Electron.* **2017**, *64*, 9001–9011. [CrossRef]
31. Zappulla, G.S.; Cougo, B.; Rodriguez Vazquez, A.L.; Russo, A.; Guida, B. Optimization of Bidirectional Modular DC/DC Converter for Low and High Power Operation in Aircraft Applications. In Proceedings of the 2021 22nd IEEE International Conference on Industrial Technology (ICIT), Valencia, Spain, 10–12 March 2021; Volume 1, pp. 458–463.
32. Khalil, H.K. *Nonlinear Systems*, 3rd ed.; Prentice-Hall: Upper Saddle River, NJ, USA, 2002; The book can be consulted by contacting: PH-AID: Wallet, Lionel.
33. Bartolini, G.; Ferrara, A.; Usai, E. Chattering avoidance by second-order sliding mode control. *IEEE Trans. Autom. Control.* **1998**, *43*, 241–246. [CrossRef]
34. Liberzon, D. *Switching in Systems and Control*; Systems & Control: Foundations & Applications; Birkhäuser: Boston, MA, USA, 2003.
35. MATLAB. Version 9.5.0 (R2018b). 2022. Available online: https://www.mathworks.com/help/releases/R2018b/physmod/sps/powersys/ref/battery.html (accessed on 15 January 2023).
36. Sumsurooah, S.; He, Y.; Torchio, M.; Kouramas, K.; Guida, B.; Cuomo, F.; Atkin, J.; Bozhko, S.; Renzetti, A.; Russo, A.; et al. ENIGMA—A Centralised Supervisory Controller for Enhanced Onboard Electrical Energy Management with Model in the Loop Demonstration. *Energies* **2021**, *14*, 5518. [CrossRef]